A Dual Frequency Tuning Method for Improved Coupling Tolerance of Wireless Power Transfer System

Zixi Liu, Mei Su, Qi Zhu, Lei Zhao, and Aiguo Patrick Hu, *Senior Member*, *IEEE*

***Abstract*—This letter proposes a dual-frequency tuning method for improved coupling tolerance of an inductively coupled wireless power transfer (WPT) system by exploiting the fundamental and 3rd order harmonic components of a square-wave voltage out of a full-bridge inverter. A dual-frequency hybrid compensation topology is designed to simultaneously utilize the characteristics of series-series (SS) and LCL-S networks under the two different frequencies. Consequently, the output power of the proposed system under a fixed load is maintained approximately constant against coupling variations. A practical hybrid WPT system with a 100 kHz square-wave excitation and a 10.5 Ω resistive load is built to verify the theoretical modelling and analysis. Experimental results show that the system achieves an approximately constant output voltage and power of around 39 V and 150 W against a coupling coefficient variation from 0.52 to 0.72, with maximum fluctuations less than 5% and 10%, respectively.**

***Index Terms*—Coupling tolerance, dual-frequency tuning, hybrid compensation, square wave excitation, wireless power transfer.**

I. Introduction

Wireless power transfer (WPT) is gaining acceptance by users in different scenarios [1-5] as a convenient and efficient technology to transfer power without direct electrical contacts, such as medical implantation [2], portable devices [3], autonomous underwater vehicle (AUV) [4] and electric vehicles (EVs) [5]. However, the requirement of alignment for a good charging performance has a negative impact on the popularization of this technology. As a result, there is a clear need for developing low-cost and reliable WPT systems with high coupling tolerances for practical applications.

Normally, additional DC-DC converters are used to compensate for the system performance degradation caused by coupling variation, which inevitably increases the size, cost, and control complexity. To improve the system coupling tolerance and reduce the demand for DC-DC converters, J Chen et al. proposed a one-to-multiple coil circuit topology to improve horizontal misalignment tolerance [6], but this system needs a multi-winding transformer and additional switches to assist the mixed-mode operation. In addition, W Tang et al. proposed a 3-dimensional (3D) WPT system with three orthogonal transmitter coils to track the receiver movement and guarantee system misalignment insensitivity at the cost of applying a complex gradient descent control algorithm [7]. L Zhao et al. proposed a hybrid WPT system by integrating series-series (SS) and LCL-LCL compensation topologies which can reduce the power fluctuation caused by 3D coil misalignment [8]-[9]. X Qu et al investigated a family of hybrid IPT topologies and achieved constant current (CC) or constant voltage (CV) output based on the input-series–output-parallel (ISOP) circuit [10]. However, these hybrid systems need more than two coils and provide limited lateral misalignment due to asymmetry pad geometry.

Except for the optimization of coil structures, some scholars focused on the research of a multi-resonant system, which is a promising way to improve the performer of the resonant converter. D Huang et al. first proposed the multi-element resonant converters and pioneered a systematic methodology to select the desired resonant topologies [11]-[12]. Further, Z Pantic et al. applied multi-frequency resonant topologies into the WPT system and demonstrated its superiors compared to the traditional single-frequency WPT system [13]. Since the correctness of the concept of the multi-frequency resonant system has been verified, further researches on this direction are carried out. For example, C Xia et al. explored the use of harmonics in inductively coupled power transmission (ICPT) systems to achieve stable power transmission [14]-[15]. But these systems have two separate frequency branches and two pairs of coils. Besides, R Mai et al. introduced a dual-resonant tank for resisting coil misalignment [16], but the calculation of transmitter currents in this system is complicated. Similarly, E Lee et al. introduced a dual-matching scheme which is robust to the distance variation [17]. However, this system needs two input sources at different frequencies, which increases the complexity of modulation and the realization of zero-phase angle (ZPA).

This work was supported in part by the Hunan Provincial Key Laboratory of Power Electronics Equipment and Grid under Grant 2018TP1001, in part by the National Natural Science Foundation of China under Grant 61933011, 61903382, in part by the Natural Science Foundation of Hunan Province, China under Grant 2020JJ5722, in part by the CRRC Zhuzhou Electric Locomotive Institute Co., Ltd. (YJYJS2018-017). *(Corresponding author: Qi Zhu).*

Zixi Liu and Mei Su are with the Hunan Provincial Key Laboratory of Power Electronics Equipment and Gird, School of Automation, Central South University, Changsha 410083, China (E-mail: zgliuzixi@163.com, sumeicsu@csu.edu.cn).

Qi Zhu, Lei Zhao, and Aiguo Patrick Hu are with the Department of Electrical, Computer, and Software Engineering, The University of Auckland, Auckland 1023, New Zealand. (e-mail: csu_zhuqi@163.com, lzha915@aucklanduni.ac.nz, a.hu@auckland.ac.nz)

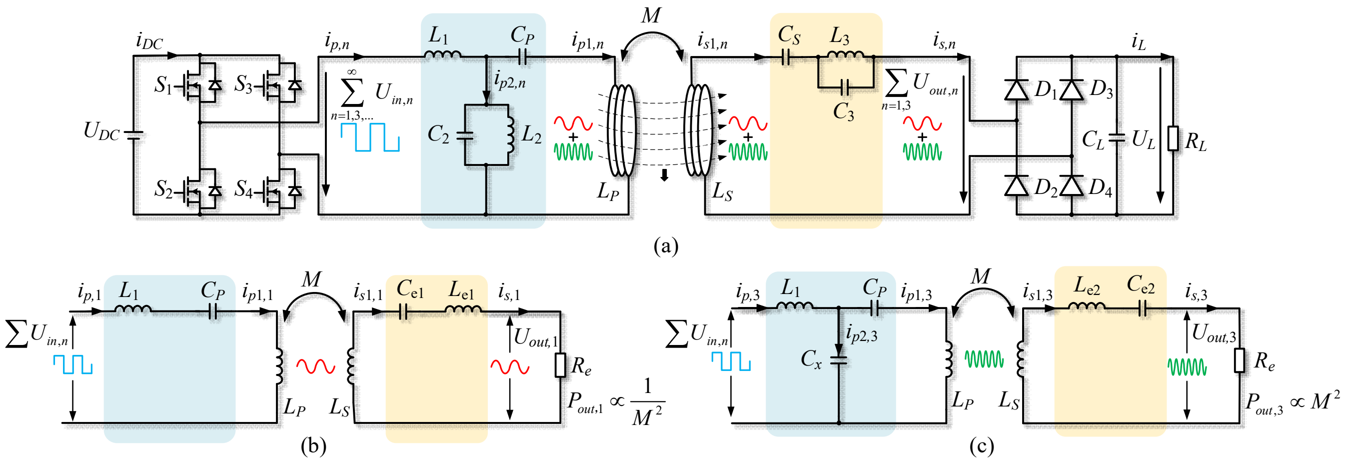

Fig. 1. Proposed hybrid WPT system with dual-frequency tuning: (a) overall structure; (b) equivalent circuit at the fundamental frequency; (c) equivalent circuit at the 3rd order harmonic frequency.

This letter proposes a dual-frequency tuning method to improve coupling tolerance for a two-coil WPT system. Such a system forms two power flow channels at both the fundamental and 3rd order harmonic frequencies of the input square-wave voltage out of a full-bridge inverter. A dual-side hybrid compensation network tuned at these two frequencies is designed to combine the power transmission characteristics of SS and LCL-S circuit topologies. The system output power fluctuation under coupling variations is significantly reduced by the compensative contributions of the two frequencies. A practical dual-frequency tuning WPT system with square-wave excitation is built to verify the proposed method.

The rest of this letter is organized as follows: the hybrid circuit topology and dual-frequency tuning method are introduced in Section II. The system modelling is established, and the voltage gain and coupling tolerance of the system are analyzed in Section III. A prototype is built, and simulation and experimental results are shown in Section IV. Finally, a conclusion is drawn.

II. Circuit Topology and Tuning Method

A. Hybrid Circuit Topology

The overall structure of the proposed hybrid WPT system is depicted in Fig. 1(a). On the left side, the DC-AC converter formed by a full-bridge is used to convert the DC voltage U_{DC} and current i_{DC} into AC voltage and current. The output AC square-wave voltage can be decomposed into the Fourier series of the fundamental and odd harmonics [13]. $U_{in,n}$ represents the nth harmonic voltage. On the right side, a rectifier and a filter capacitor C_L are used to rectify the output voltage $U_{out,n}$ into the DC voltage U_L to power the load R_L.

The shaded parts of Fig. 1(a) show the hybrid compensation networks tuned at two tuning frequencies. The primary circuit consists of two sets of LC branches: the series LC, consisting of L_1 and C_P, and the parallel LC, consisting of L_2 and C_2. The secondary circuit is formed by a capacitor C_S, and a parallel LC consisting of L_3 and C_3. M is the mutual inductance between L_P and L_S. This hybrid compensation network will show different circuit characteristics at the fundamental f_1 and 3rd order harmonic frequencies f_3. As shown in Fig. 1(b), L_1, C_P, and L_P form a series resonant tank which allows the fundamental current to go through the transmitter coil. As shown in Fig. 1(c), C_2 and L_2 are used to form a parallel resonant tank with L_P to preserve the 3rd order harmonic current and allow it to go through the transmitter coil. These two current components in the transmitter coil generate two magnetic fields at different frequencies. Both the magnetic fields are coupled to the receiver coil, so power can be transferred to the secondary side by electromagnetic induction. L_S, C_S, L_3, and C_3 form two series resonant networks, which enable power flow via two frequency channels.

B. Dual Frequency Tuning Method

The component parameters of the proposed hybrid circuit should be designed to meet some constraints to realize dual-frequency power transmission. First, when only considering the fundamental component of the square-wave voltage, the parameter values should satisfy (1) where ω_1 is the angular frequency of f_1.

$$\begin{cases} \omega_1^2 L_2 C_2 = 1 \\ \omega_1^2 (L_1 + L_P) C_P = 1 \\ \omega_1^2 L_{e1} C_{e1} = 1 \end{cases} \tag{1}$$

where

$$j\omega_1 L_S + \frac{1}{j\omega_1 C_S} = \frac{1}{j\omega_1 C_{e1}}, \quad \frac{j\omega_1 L_3}{1-\omega_1^2 L_3 C_3} = j\omega_1 L_{e1}.$$

At the fundamental frequency, L_2 and C_2 are in the parallel resonant which is equivalent to an open circuit. Therefore, the whole circuit can be simplified as shown in Fig. 1(b), which is equivalent to the topology of a SS compensated WPT system. R_e is the equivalent input resistance of the rectifier, where $R_e = 8R_L/\pi^2$. $P_{out,1}$ is the active power generated by the fundamental voltage.

Similarly, when only considering the 3rd order harmonic component, the parameter values should satisfy (2) where ω_3 is the angular frequency of f_3.

$$\begin{cases} \omega_3^2 L_1 C_x = 1 \\ \omega_3^2 L_{P2} C_x = 1 \\ \omega_3^2 L_{e2} C_{e2} = 1 \end{cases} \tag{2}$$

where

$$\frac{j\omega_3 L_2}{1-\omega_3^2 L_2 C_2} = \frac{1}{j\omega_3 C_x},\ j\omega_3 L_P + \frac{1}{j\omega_3 C_P} = j\omega_3 L_{P2},$$

$$j\omega_3 L_S + \frac{1}{j\omega_3 C_S} = j\omega_3 L_{e2},\ \frac{j\omega_3 L_3}{1-\omega_3^2 L_3 C_3} = \frac{1}{j\omega_3 C_{e2}}.$$

At the 3rd order harmonic frequency, the proposed system can be simplified to an equivalent circuit shown in Fig. 1(c), which is equivalent to the topology of an LCL-S compensated WPT system. $P_{\text{out},3}$ is the active power generated by the 3rd order harmonic voltage. In general, when both equations (1) and (2) are satisfied, $P_{\text{out},1}$ and $P_{\text{out},3}$ will contribute to the total output power at the same time.

C. Voltage Gain and Zero Phase Angle

The voltage gain-frequency curves of the hybrid compensation network and the phase-frequency curves of the inverter output current are shown in Fig. 2. f_0 is the fundamental resonant frequency of the hybrid compensation network, f_s is the operating frequency. V_{out} and V_{in} are the output and input voltages. The voltage gain is denoted by V_{out}/V_{in} . i_{p} is the output current of the inverter.

It can be seen from Fig.2(a) that the proposed system has two resonant points at f_0 and $3f_0$, and the voltage gain decreases with the increases of k at f_0, while increases with the increases of k at $3f_0$. Furthermore, Fig. 2(b) shows that the phase angle of the inverter current is around zero at f_0 and $3f_0$, which indicates the proposed circuit has achieved zero-phase angle (ZPA) at the two resonant points, which provides a good base for soft switching operation of the voltage fed inverter.

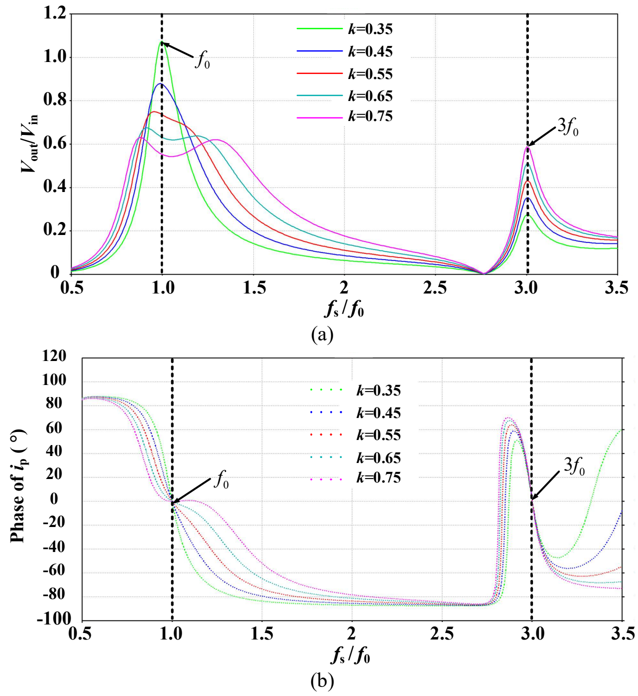

Fig. 2 Voltage gain and inverter current phase angle curves of the proposed hybrid compensation network versus frequency.

III. System Modelling and Coupling Tolerance Analysis

A. System Mathematical Modelling

Based on the circuit topology and dual-frequency tuning method, the proposed system can be mathematically modelled as follows.

$$\begin{bmatrix} U_{in,n} \\ 0 \\ 0 \end{bmatrix} = \begin{bmatrix} Z_{11} & Z_{12} & Z_{13} & Z_{14} \\ Z_{21} & Z_{22} & Z_{23} & Z_{24} \\ Z_{31} & Z_{32} & Z_{33} & Z_{34} \end{bmatrix} \begin{bmatrix} i_{p,n} \\ i_{p1,n} \\ i_{p2,n} \\ i_{s1,n} \end{bmatrix} \quad n = 1,3 \tag{3}$$

where

$$Z_{11} = j\omega_n L_1 + r_1,\ Z_{12} = 0,\ Z_{13} = \frac{j\omega_n L_2 + r_2}{1-\omega_n^2 L_2 C_2 + j\omega_n C_2 r_2},\ Z_{14} = 0,$$

$$Z_{21} = 0,\ Z_{22} = j\omega_n L_P + r_P + \frac{1}{j\omega_n C_P},\ Z_{23} = -\frac{j\omega_n L_2 + r_2}{1-\omega_n^2 L_2 C_2 + j\omega_n C_2 r_2},$$

$$Z_{24} = -j\omega_n M,\ Z_{31} = 0,\ Z_{32} = -j\omega_n M,\ Z_{33} = 0,$$

$$Z_{34} = j\omega_n L_S + r_S + \frac{1}{j\omega_n C_S} + \frac{j\omega_n L_3 + r_3}{1-\omega_n^2 L_3 C_3 + j\omega_n C_3 r_3} + R_e.$$

r_{P} and r_s are the parasitic resistances of transmitter and receiver coils. r_i (i=1,2,3) is the parasitic resistance of inductor L_i. The subscript n denotes the parameters regarding the fundamental and 3rd order harmonic frequencies. Equation (3) describes the electrical behaviors of the hybrid system under different exciting frequencies.

By ignoring copper losses and assuming the system is well-tuned at both frequencies, the currents in the transmitter and receiver coils can be simplified by substituting (1) and (2) into (3).

$$\begin{aligned} i_{p1,1} &= \frac{U_{in,1}}{\omega_1^2 M^2} R_e, \quad & i_{s1,1} &= \frac{jU_{in,1}}{\omega_1 M} \\ i_{p1,3} &= \frac{U_{in,3}}{j\omega_3 L_1}, \quad & i_{s1,3} &= \frac{M}{L_1 R_e} U_{in,3} \end{aligned} \tag{4}$$

where $i_{\text{p1,1}}$, $i_{\text{p1,3}}$, and $i_{\text{s1,1}}$, $i_{\text{s1,3}}$ are the fundamental and 3rd order harmonic currents in the transmitter and receiver coils, respectively.

B. Coupling Tolerance Analysis

The coupling variation between coils, which can be manifested as the mutual inductance variation, is mainly caused by lateral and longitudinal misalignment, and vertical distance variation [9]. Hence, the coupling tolerance of the system can be regarded as the capability of stabilizing power transmission against the mutual inductance variation. As mentioned in [13], the RMS values of the first and 3rd order harmonic voltages are defined as

$$\begin{aligned} U_{in,1}(\omega = \omega_1) &= \frac{2\sqrt{2}U_{DC}}{\pi} \\ U_{in,3}(\omega = \omega_3) &= \frac{2\sqrt{2}U_{DC}}{3\pi} \end{aligned} \tag{5}$$

Referring to [18], the active output power contributed by the fundamental and 3rd order harmonic components can be added up directly to get the total output power.

$$P_{out} = \sum_{n=1,3} V_{out,n} I_{s,n} \cos\theta_{s,n} = \sum_{n=1,3} I_{s,n}^2 R_e \tag{6}$$

where $V_{out,n}$, $I_{s,n}$ are the root-mean-square (RMS) values of $U_{out,n}$ and $i_{s,n}$, respectively. $\theta_{s,n}$ is the phase angle between $U_{out,n}$ and $i_{s,n}$ which equals zero when the load is resistance.

The output power can be calculated by substituting (4) and (5) into (6).

$$P_{out}=P_{out,1}+P_{out,3}=\frac{4U_{DC}^2}{\pi^2}\left(\frac{1}{\omega_1^2}\frac{R_e}{M^2}+\frac{1}{9L_1^2}\frac{M^2}{R_e}\right) \tag{7}$$

In (7), the active power $P_{\mathrm{out},1}$ increases with the decrease of the square of mutual inductance M^2, which is consistent with SS compensated WPT system. On the contrary, $P_{\mathrm{out},3}$ decreases with the decrease of M^2, which is consistent with LCL-S compensated WPT system. If the parameters of the proposed system are properly designed, the active output power P_{out} can maintain nearly constant, as the effect of mutual inductance variation is cancelled out by the combination of $P_{\mathrm{out},1}$ and $P_{\mathrm{out},3}$. In addition, it can be inferred from (7) that the effect of load R_e variation on the active output power P_{out} can also be cancelled out by the combination of $P_{\mathrm{out},1}$ and $P_{\mathrm{out},3}$. However, the realization of an expected load variation tolerance is also depended on the system parameter design. Moreover, the range of k with a nearly constant output power is adjustable by designing the system parameters.

C. Theoretical Coupling Coefficient Variation Range

To explain the applicable coupling range of the proposed method, equation (7) is rewritten as follows:

$$P_{out}=\frac{4U_{DC}^2L_PL_S}{9\pi^2L_1^2R_e}k^2+\frac{4U_{DC}^2R_e}{\pi^2\omega_1^2L_PL_S}\frac{1}{k^2}=Ak^2+\frac{B}{k^2} \tag{8}$$

where $A=\frac{4U_{DC}^2L_PL_S}{9\pi^2L_1^2R_e}$, $B=\frac{4U_{DC}^2R_e}{\pi^2\omega_1^2L_PL_S}$ and $k=\sqrt{L_PL_S}$.

The applicable coupling range can be studied by finding the suitable A and B to make the curve of P_{out} fall within a defined range over the expected range of k. Assume the maximum and minimum coupling coefficients are k_{max} and k_{min}, and the power fluctuation desired is within ΔP, the following bound about A and B can be obtained:

$$\left|Ak_{\max}^2+\frac{B}{k_{\max}^2}-\left(Ak_{\min}^2+\frac{B}{k_{\min}^2}\right)\right|\le\Delta P \tag{9}$$

The relationship to illustrate the bound on other circuit parameters defined by A and B is graphically shown in Fig. 3.

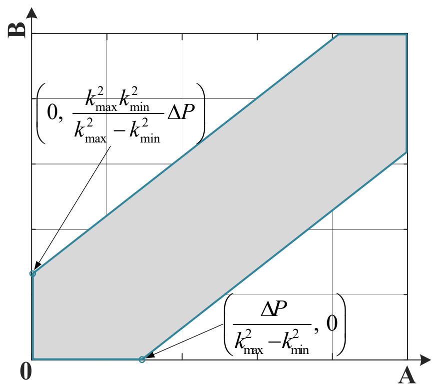

Fig. 3 Bound on other circuit parameters defined by A and B for achieving the desired output power fluctuation against coupling variations.

IV. Experimental Results

A full 150 W two-coil hybrid WPT system is designed and built as shown in Fig. 4. The experimental parameters of the system are designed to achieve dual-frequency tuning under the constraints of (1) and (2) are shown in Table I. The radii of the transmitter and receiver coils are 90 mm and 80 mm, respectively. The PWM signals driving the inverter with a phase shift angle of 90° are generated by a DSP controller of TMS320F28069, and a full-bridge diode rectifier is used to drive a DC resistive load. The switching frequency is 100 kHz.

The radial misalignment is varied from 0 to 30 mm with a fixed 3 mm vertical distance, corresponding to a coupling coefficient k variation from 0.72 to 0.52. The same range of coupling variation can also be achieved by changing the vertical distance between the two coils from 3mm to 14.7 mm.

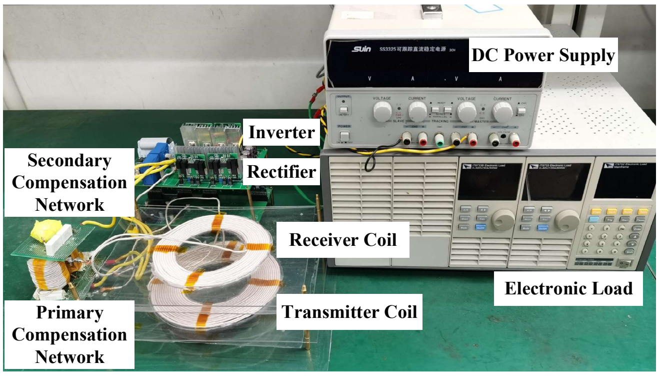

Fig. 4 Experimental setup of a 150 W prototype.

TABLE I
PARAMETERS OF THE PROPOSED HYBRID WPT SYSTEM

Parameter	Value	ESR
L_1	34.98 μH	411.9 mΩ
L_2	271.0 μH	772.4 mΩ
C_2	9.16 nF	51.0 mΩ
C_P	30.45 nF	15.3 mΩ
L_P	42.74 μH	574.5 mΩ
L_S	22.35 μH	313.5 mΩ
C_S	96.0 nF	21.3 mΩ
L_3	3.37 μH	22.7 mΩ
C_3	98.0 nF	21.3 mΩ
C_L	188.0 μF	---
R_L	10.5 Ω (IT8733B, Electronic Load)	
U_{DC}	0-60 V (SS3323, DC Power Supply)	
Inverter Switch	IPP023N10N5	
Rectifier Switch	UF3C065040K3S	

Fig. 5 shows the experimental waveforms of the inverter output voltage and current U_{in} and i_{p}, and the transmitter and receiver currents i_{p1} and i_{s1} under two coupling conditions. It can be seen from Fig. 5 (a) and (c) that the 3rd order harmonic component has a higher effect on the current waveforms under a closely coupled condition (k=0.72) than a loosely coupled condition (k=0.52). This is consistent with theoretical analysis by (4), which indicates that the 3rd order harmonic component has more contribution to power flow at the stronger magnetic coupling. Moreover, Fig. 5 (b) and (d) shows the detailed waveforms of the inverter output voltage and current which are approximately kept in phase.

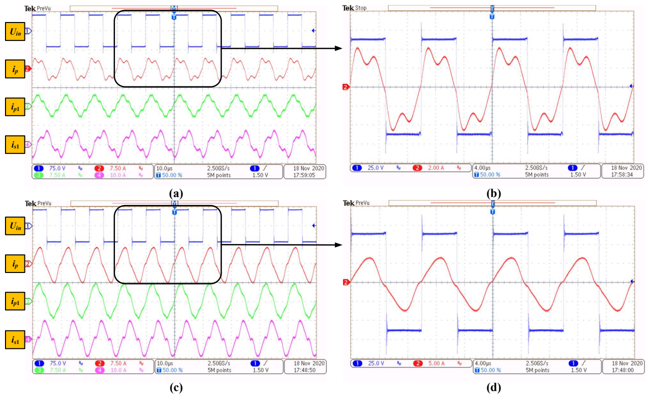

Fig. 5 Experimental overall and detailed waveforms of the output voltage and current of the inverter under different coupling coefficient: (a) overall waveforms when k=0.72; (b) detailed waveforms when k=0.72; (c) overall waveforms when k=0.52; (d) detailed waveforms when k=0.52.

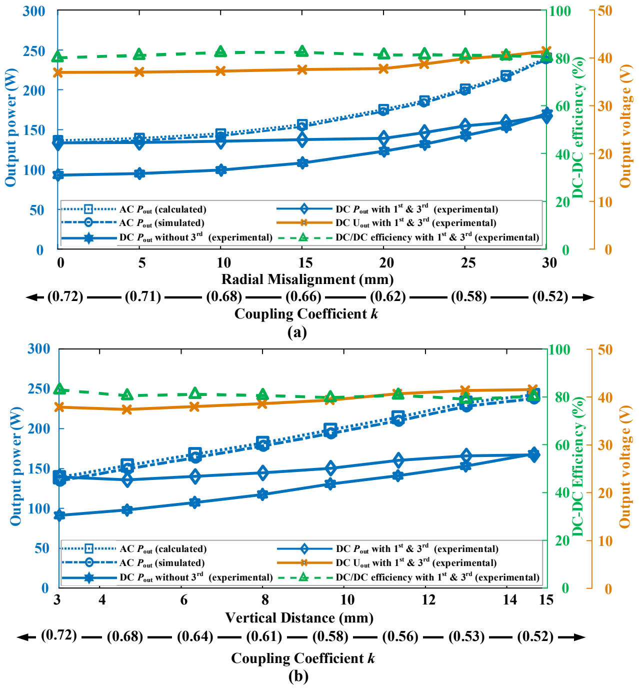

Fig. 6 Experimental DC output voltage, power and DC-DC efficiency, baseline experimental DC output power without 3rd harmonics, and calculated and simulated AC output power under coupling variations: (a) radial misalignment; (b) vertical distance change.

Fig. 6 shows experimental DC output voltage, power and DC-DC efficiency of the built IPT prototype under coupling variations caused by both radial misalignment and vertical distance change. For comparison, the theoretical and simulated output powers under ideal fundamental and 3rd order harmonic AC voltage excitations and an equivalent AC resistive load are also shown in the same figure. The experimental DC output power of a single frequency SS system tuned with the same pair of coils at the fundamental frequency is also added as the baseline for comparison. It can be seen that the theoretical and simulation results are in a very good agreement, which verifies the theoretical modelling and analysis. Due to the compensative effect against the mutual inductance variation indicated by (7), the AC output power tends to keep constant in the strongly coupled region, but it increases when the coupling gets weaker. Fig. 6 shows the experimental output power is lower than the theoretical and simulation results because of the power losses of the converters and parasitic components, and the inaccurate practical tuning. Practical losses increase with the decrease of the coupling due to higher currents, which lead to a power efficiency drop of around 4%. However, the DC output voltage and power remain approximately constant around 39 V and 150 W with maximum fluctuations of 5% and 10%, respectively, which is much smaller than the theoretical prediction and practical baseline.

V. CONCLUSION

This letter proposed a dual-frequency tuning method to improve the coupling tolerance of an inductively coupled WPT system. This system makes use of both the fundamental and 3rd order harmonic components of the input square-wave voltage from a full-bridge inverter for wireless power transfer across the same magnetic coupling channel by two coupled coils. Through the dual-resonant-frequency compensation network, the output power is kept approximately constant against coupling variations due to the compensative contributions of the fundamental and 3rd harmonic components. The experimental results demonstrated that the proposed hybrid system can achieve smooth output voltage and power of around 39 V and 150 W with maximum fluctuations within 5% and 10% against a coupling coefficient variation between 0.52 and 0.72. Future research will include system parameter optimization and system efficiency improvement.

REFERENCES

[1]. Z Zhang, H Pang, et al, “Wireless Power Transfer—An Overview”, IEEE Transactions on Industrial Electronics, vol. 66, no. 2, pp. 1044-1058, Fed. 2019.
[2]. P Si, A P Hu, S Malpas, et al. "A frequency control method for regulating wireless power to implantable devices," IEEE transactions on biomedical circuits and systems, vol. 2, no. 1, pp. 22-29, Apr 2008.
[3]. E S. Lee, B H. Choi, Y H. Sohn, et al, “Multiple dipole receiving coils for 2-D omnidirectional wireless mobile charging under wireless power zone”, 2015 ECCE, Montreal, QC, Canada, Sep. 20-24, 2015.
[4]. T Kan, R Mai, P P Mercier, et al, “Design and analysis of a three-phase wireless charging system for lightweight autonomous underwater vehicles”. IEEE Transactions on Power Electronics, vol. 33, no. 8, pp. 6622-6632, Sep 2017.
[5]. S Li, C C Mi, “Wireless power transfer for electric vehicle applications”, IEEE journal of emerging and selected topics in power electronics, vol. 3, no. 1, pp. 4-17, Mar 2015.
[6]. J Chen, H Zhou, Q Deng, et al, “Free-Positioning Wireless Power Transfer System Based on One-to-Multiple Topology”, IEEE Transactions on Power Electronics, vol. 35, no. 10, pp. 9959-9964, Feb 2020.
[7]. W Tang, Q Zhu, J Yang, et al. “Simultaneous 3-D Wireless Power Transfer to Multiple Moving Devices with Different Power Demands”, IEEE Transactions on Power Electronics, vol. 35, no. 5, pp. 4533 – 4546, Sep 2019.
[8]. L Zhao, D J Thrimawithana, U K Madawala, “Hybrid bidirectional wireless EV charging system tolerant to pad misalignment”, IEEE Transactions on Industrial Electronics, vol. 64, no. 9, pp. 7079-7086, Mar 2017.
[9]. L Zhao, D J Thrimawithana, U K Madawala, et al, “A Misalignment-Tolerant Series-Hybrid Wireless EV Charging System with Integrated Magnetics”, IEEE Transactions on Power Electronics, vol. 34, no. 2, pp. 1276-1285, Apr 2018.
[10]. X Qu, Y Yao, D Wang, et al, “A Family of Hybrid IPT Topologies With

Near Load-Independent Output and High Tolerance to Pad Misalignment", IEEE Transactions on Power Electronics, vol. 35, no. 7, pp. 6867-6877, Jul. 2020.
[11]. D Huang, P Kong, F C. Lee, et al, "A Novel Integrated Multi-Elements Resonant Converter", 2011 IEEE ECCE, Phoenix, AZ, USA, Sep, 17-22, 2011.
[12]. D Huang, F. C. Lee, D Fu, "Classification and Selection Methodology for Multi-element Resonant Converters", 2011 26th APEC, Fort Worth, TX, USA, Mar 6-11, 2011.
[13]. Z Pantic, K Lee, S M. Lukic, "Multifrequency Inductive Power Transfer", IEEE Transactions on Power Electronics, vol. 29, no. 11, pp. 5995 – 6005, Jan 2014.
[14]. C Xia, R Jia, Y Wu, et al, "WPIT technology based on the fundamental harmonic component for a single-channel and two-coil ICPT system", IET Power Electronics, vol. 12, no. 10, pp. 2608-2614, Aug 2019.
[15]. C Xia, S Ren, N Ma, et al, "Inductively Coupled Power Transfer System with Fundamental Wave and Harmonic Wave Two-path Parallel Transmission", Automation of Electric Power Systems, vol. 41, no. 7, pp. 93-100, Apr 2017.
[16]. R Mai, Z Yan, Y Chen, et al, "A Hybrid Transmitter Based Efficiency Improvement Controller with Full-Bridge Dual Resonant Tank for Misalignment Condition", IEEE Transactions on Power Electronics, vol. 35, no. 1, pp. 1124-1135, May 2019.
[17]. E Lee, W Kang, H Ku. "A Magnetic Resonance Wireless Power Transfer System Robust to Distance Variation Using Dual-Matching Scheme", Journal of Electrical Engineering & Technology, vol. 14, no. 1, pp. 2097-2103, Aug 2019.
[18]. C Li, Z Bai, X Xiao, et al, "Research of harmonic distortion power for harmonic source detection", 2016 17th ICHQP, Belo Horizonte, Brazil, Oct. 16-19, 2016.